Hindawi
Journal of Chemistry
Volume 2019, Article ID 8587949, 10 pages
https://doi.org/10.1155/2019/8587949

Research Article

Preparation of Highly Stable and Effective N-Doped TiO_2@SiO_2 Aerogel Catalyst for Degradation of Organic Pollutants by Visible Light Catalysis

Shiyun Tang,[1,2] **Jingyu Ran**,[1,2] **Junjiang Guo**,[1,2] **and Anjiang Tang**[1,2]

[1]*College of Chemical Engineering, Guizhou Institute of Technology, Guiyang 550003, China*
[2]*Engineering Technology Research Center of Fluorine Silicon Material, Guiyang 550003, China*

Correspondence should be addressed to Shiyun Tang; 524506512@qq.com

Received 20 July 2019; Revised 7 October 2019; Accepted 15 October 2019; Published 3 November 2019

Guest Editor: Fada Feng

To obtain high stable and effective TiO_2 photocatalyst, nano-N-doped TiO_2@SiO_2 ($TiO_{2-x}N_x$@SiO_2, $0 \le x \le 2$) composite aerogels were synthesized by the sol-gel method combined with supercritical drying and direct oxidation process. The adsorption/photocatalytic degradation efficiency of $TiO_{2-x}N_x$@SiO_2 aerogels was evaluated by the degradation of RhB in aqueous solution under visible light irradiation. The physiochemical properties of the aerogels were examined by XRD, FT-IR, TEM, SEM, TG/DTA, and BET methods. It was found that the specific surface areas of all $TiO_{2-x}N_x$@SiO_2 samples exceeded 700 m^2/g and exhibited a honeycomb porous structure with fine particulate morphology. Photocatalytic activity tests show that the 500-TiO_2@SiO_2 composite aerogel exhibits the best adsorption/photocatalytic degradation rate for RhB, which obtained about 80% of the degradation rate in 30 min under visible light and over 95% after 120 min. On the one hand, the SiO_2 aerogels can significantly inhibit the phase transition of TiO_2, and the nano TiO_2 can be highly dispersed in the SiO_2 aerogels; On the other hand, if the oxidation temperature is selected properly, the N-doped $TiO_{2-x}N_x$@SiO_2 aerogel can be obtained by simple TiN@SiO_2 aerogel oxidation.

1. Introduction

Titanium oxide (TiO_2) is an excellent semiconductor photocatalyst because of its high photocatalytic activity, good chemical stability, safety, nontoxicity, and low cost without secondary pollution [1–3]. In the past decades, TiO_2 as photocatalytic materials has become the important subject of attention by many researchers at home and abroad, in the water/air treatment [4], solar cell electrodes [5], water decomposition for hydrogen production [6], and other fields. It has three polymorphs in nature: anatase, rutile, and brookite. The main photocatalytic activities are anatase and rutile TiO_2. Rarely researchers focus on brookite TiO_2 due to its little photocatalytic activity and low thermal stability [7]. However, owing to the rather high intrinsic bandgap of pure TiO_2 (about 3.0 eV), only 3%–5% of the incoming solar energy on the earth's surface can be utilized. Many problems still restrict the practical application of TiO_2 as a photocatalyst with excellent performance, such as low quantum efficiency, narrow light absorption wavelength, low solar energy utilization, and poor adsorption and recycling in the suspended phase photocatalytic system of water treatment.

To improve the photocatalytic efficiency of TiO_2, an extensive interest is invested in the use of metal or nonmetal as dopant during the preparation process. This principle is based on the "band filling mechanism;" the bandgap energy can be increased by doping metallic ions or nonmetallic element because the photoexcited electrons can be confined in the conduction band; thus, their lifetime can be prolonged [8]. Although metal and nonmetallic ion modification methods can improve the performance of TiO_2 photocatalyst to some extent, TiO_2 doped with metal ions is often thermounstable and the carrier recombination rate increases, thus sacrificing its photocatalytic ability in the ultraviolet

(UV) region. On the contrary, TiO_2 doped with nonmetallic can not only enhance the visible light response ability but also maintain the photocatalytic activity in the UV region. Therefore, the nonmetallic ions doping in TiO_2 photocatalyst has shown great industrial application prospects. At present, the research studies on doping of nonmetallic ions are mainly focused on C [9], N [10], S [11], and F [12]. Among them, N is easy to be introduced into the structure of TiO_2 because of the comparable atomic radius to O atom, low ionization energy, and high stability. N-doped TiO_2 composite oxides always use the concentrated $NH_3{\cdot}H_2O$ or NH_4F as nitrogen and fluorine source [13]. The photocatalytic activity of TiO_2 can be significantly improved with the addition of N [14, 15]. Therefore, N-doped TiO_2 has become the most promising doping method for nonmetallic doping.

Moreover, to obtain the high-performance photocatalyst, nanosized TiO_2 is often used due to the higher photocatalytic activity than ordinary TiO_2. Nevertheless, TiO_2 nanoparticles tend to aggregate, which reduce its efficiency. To solve this problem, this work employs the SiO_2 aerogel as a support for TiO_2 nanoparticles, which make TiO_2 nanoparticles highly dispersed in SiO_2 aerogels, thus preventing its aggregation. SiO_2 aerogel is a solid material composed of nanoparticles or polymer molecules, which are crosslinked to form nanoporous skeleton structure. The unique nanoscale skeleton and pore distribution feature endow its excellent performance, such as ultralow density (as low as 0.003 g/cm^3), high porosity (above 90%), huge specific surface area (500–1200 m^2/g), strong transmittance (about 93%), low refractive index, and small dielectric constant (<1.01) [16–18]. Owing to these characteristics, SiO_2 aerogel has a broad application prospect in the field of thermal insulation materials, sound insulation materials, filter materials, catalysts, adsorbents, sensors, fuel cells, etc. [19–21].

It is important to combine the excellent properties of aerogels with nanophotocatalysts to take full advantage of the high adsorption efficiency and strong transmittance of SiO_2 aerogel and photocatalytic activity of nanosized TiO_2 photocatalyst simultaneously. The nano-TiN@SiO_2 composite aerogel materials were prepared by the sol-gel method combined with supercritical drying process. Then, the nano-N-doped TiO_2@SiO_2 ($TiO_{2-x}N_x$@SiO_2, $0 \le x \le 2$) composite aerogels were obtained by the direct oxidation method. Finally, the adsorption/photocatalytic degradation efficiency for Rhodamine B (RhB) in aqueous solution of the $TiO_{2-x}N_x$@SiO_2 composite aerogels have been analyzed and discussed. This preparation process of aerogels can be either supercritical drying or ambient pressure drying [22, 23], and it can be easily scaled up for industrial production of visible light-driven N-doped TiO_2 photocatalyst for pollutants removal because of its convenience and energy-saving properties.

2. Experimental Details

2.1. Materials. Nano-TiN powder (≥99.9%) with a particle size of 20 nm and density of 5.24 g/cm^3 was purchased from Shanghai Aladdin Biochemical Technology Co., Ltd. Tetraethoxysilane (TEOS), absolute ethanol (C_2H_5OH), hydrochloric acid (HCl), ammonia ($NH_3{\cdot}H_2O$), and RhB were obtained from ScienceLab Instrument Inc., Guizhou. All the reagents were of analytical grade purity and used without further purification. Deionized water was used throughout the experiment.

2.2. Preparation of $TiO_{2-x}N_x$@SiO_2 Composite Aerogel. Nano-TiN@SiO_2 composite aerogel was synthesized through the sol-gel method with the high-temperature supercritical drying. The procedure is as follows: Firstly, a certain amount of C_2H_5OH and TEOS were put into water (The volume ratio of C_2H_5OH : TEOS : H_2O is 1 : 3 : 6) and dispersed by ultrasonic oscillation for 30 min at room temperature. Then, adding 1 mol/L HCl as catalyst, adjusting pH value to 1.5–2.5 under magnetic stirring for 2 hours, followed by addition of 0.2 mol/L $NH_3{\cdot}H_2O$ slowly until the pH value is 7-8. At the same time, appropriate amount of nano-TiN powder (the theoretical wt.% of TiN is 10%) was added rapidly under intense stirring. The solution was continuously stirred for 2.5 h and subsequently aged for 2 h to obtain TiN@SiO_2 gel with appropriate viscosity. Prior to supercritical drying, the gel was soaked in ethanol for 4-5 times, and the aging solution was replaced every 24 h. Finally, the gel was transferred to an autoclave with admitting nitrogen gas into the chamber at about 2 MPa. Heating was carried out at a rate of 1°C/min until 260°C. This was chosen as the supercritical temperature for the ethanol solvents and the necessity to avoid any thermal decomposition of the solvent. The pressure inside the autoclave gradually increases to about 8 MPa when the supercritical temperature was achieved. The final pressure and temperature were maintained for at least 15 min. After that, the solvent was rapidly removed by opening the outlet valve to vent, and the autoclave was then allowed to cool to room temperature and disassembled. A black-colored aerogel powder of TiN@SiO_2 was obtained at this stage. To gain the $TiO_{2-x}N_x$@SiO_2 composite aerogel, the TiN@SiO_2 was ground into a finer powder and calcinated at the fixed temperature for 2 h in a furnace under air atmosphere. The samples were coded as calcinated temperature- TiO_2@SiO_2, e.g., the TiN@SiO_2 aerogels calcined at 300°C were recorded as 300-TiO_2@SiO_2. Color changed from black to light yellow N-doped TiO_2@SiO_2 ($TiO_{2-x}N_x$@SiO_2, $0 \le x \le 2$) composite aerogels after different temperature calcined.

2.3. Photocatalytic Activity Evaluation. The photocatalytic activity of $TiO_{2-x}N_x$@SiO_2 composite aerogel was evaluated by the degradation of RhB in aqueous solution under simulated solar irradiation with a 500 W Xenon lamp (Beijing Perfectlight Technology Co. LTD., PLS-SXE300/300 UV). The lamp was positioned inside a cylindrical vessel and surrounded by a circulating water jacket to cool it. An amount of 10 mg photocatalyst was totally suspended in a 100 ml aqueous solution of 10 mg·L^{-1} RhB. The solution was treated by ultrasonic oscillation for 15 min at room temperature. Then, the solution was shined with visible light by removing ultraviolet light using a filter. The distance

between light source and the bottom of the solution was about 15 cm. At each time interval, 4 ml of the suspension was extracted for analysis during each photocatalytic process. Finally, the concentration of RhB was monitored by colorimetry with a UV-Vis spectrophotometer (Lambda35, PerkinElmer) at its maximum absorption wavelength. The adsorption/photocatalytic degradation efficiency of RhB was defined according to the following equation:

$$\eta(\%) = \frac{(C_0 - C_t)}{C_0} * 100\%, \quad (1)$$

where η is the adsorption/photocatalytic degradation rate, C_0 was the initial concentration of RhB, and C_t was the corresponding concentration of RhB at certain reaction time.

2.4. Characterization. The specific surface area and pore size distribution of aerogels were determined by the Brunauer–Emmitt–Teller N_2 adsorption-desorption method (BET, HYA2010-B1). Pore size distribution and specific desorption pore volumes were obtained using the Barrett-Joyner-Halenda (BJH) method using the desorption branches. The surface morphology and porous structure of aerogel photocatalysts were observed by scanning electron microscopy (SEM, Nova Nano 450, FEI, USA) and transmission electron microscopy (TEM, Tecnai G^2 F20 S-TWIN, FEI, USA). The phase compositions of the samples were determined by X-ray diffraction analysis (XRD, Ultima IV, Rigaku Corporation, Japan), which was carried out in a DX-2500 rotating anode X-ray diffractometer using Cu $K\alpha$ ($\lambda = 0.15406$ nm) radiation within the 2θ range of 10–80°. Thermogravimetric and differential thermal analysis (TG/DTA, Beijing Everlasting Scientific Instrument Factory, ZH-1450) were performed in air atmosphere at a heating rate of 10°C/min from the room temperature to 750°C. Fourier transform infrared (FT-IR) spectra were recorded on a Spectrum VERTEX 80 spectrometer in the range of 400–4000 cm^{-1}.

3. Results and Discussion

3.1. Morphology and Structures of Composite Aerogels. The N_2-BET is used to characterize the porosity and surface area of the as-prepared TiN@SiO_2 and $TiO_{2-x}N_x$@SiO_2 composite aerogels. A typical nitrogen adsorption-desorption isotherm and pore size distribution of TiN@SiO_2 composite aerogel is presented in Figure 1. According to IUPAC classification, the adsorption isotherm of TiN@SiO_2 aerogel corresponds to type-IV, which is considered to be due to the presence of mesopores in aerogel. The pore shape can be identified by the hysteresis loop, the TiN@SiO_2 aerogel shows the type-H2 hysteresis loop in relative pressure (P/P_0) ranges from 0.70 to 0.98, which suggests that the pore structures are complex and tend to be made up of interconnected networks with different sizes and shapes. Furthermore, the illustration of Figure 1 shows the pore size distributions measured by the BJH model. It is evident that there is a bimodal distribution, which was concentrated at 9.90 nm and 13.21 nm, respectively.

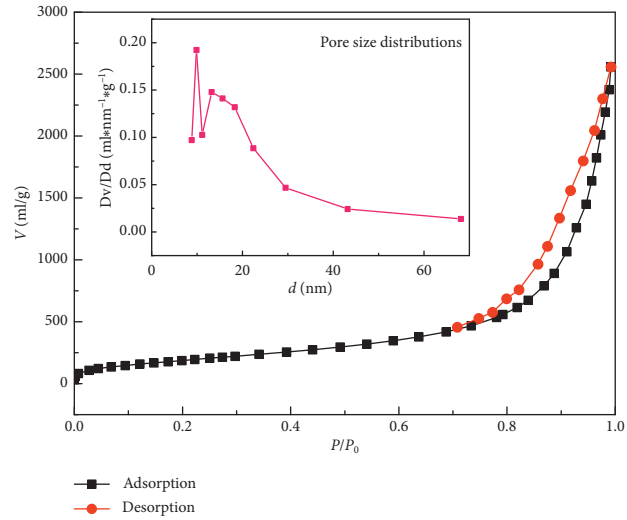

Figure 1: Adsorption-desorption isotherm and pore size distribution of TiN@SiO_2 composite aerogel.

Table 1: Specific surface area (S_{BET}), average diameter (d), and mesopore volume (V_p) of the aerogel samples.

Sample	S_{BET} (m^2/g)	d (nm)	V_p (cm^3/g)
As-prepared TiN@SiO_2	711	16.32	4.19
300-TiO_2@SiO_2	743	12.97	3.18
500-TiO_2@SiO_2	770	11.29	2.85
700-TiO_2@SiO_2	703	12.66	2.93

The specific surface areas of as-prepared TiN@SiO_2, 300-TiO_2@SiO_2, 500-TiO_2@SiO_2, and 700- TiO_2@SiO_2 composite aerogels are listed in Table 1. All samples were porous and developed a huge specific area (exceed 700 m^2/g). Specifically, the specific surface of the as-prepared TiN@SiO_2 aerogel sample is 711 m^2/g and slightly increases reaching about 743 m^2/g after thermal oxidation at 300°C for 2 h, then further increased to 770 m^2/g after calcined at 500°C for 2 h. However, the specific surface of 700-TiO_2@SiO_2 aerogel decreases to 703 m^2/g as expected. It can be seen that the composite aerogels manage to preserve a substantial specific surface even with calcination at 700°C. The average diameters of the pores obtained by BET analysis are 16.32 nm for as-prepared TiN@SiO_2, 12.97 nm for 300-TiO_2@SiO_2, 11.29 nm for 500-TiO_2@SiO_2, and 12.66 nm for 700-TiO_2@SiO_2, and the corresponding mesopore volumes are 4.19 cm^3/g, 3.18 cm^3/g, 2.85 cm^3/g, and 2.93 cm^3/g, respectively. It is obvious that the pore size of aerogels is relatively stable after calcination, which means that the aerogels have the high thermal stability.

SEM and TEM images are presented in Figure 2 for a few structural characteristic TiN@SiO_2 composite aerogel before and after thermal treatment. The SEM image of the as-prepared TiN@SiO_2 sample is shown in Figure 2(a). It can be seen that it exhibits a honeycomb porous structure with fine particulate morphology. The structure is quite uniform and amorphous flocculent on the whole. However, the accurate determination of crystallite size cannot be made by SEM. This was subsequently observed by using the TEM image

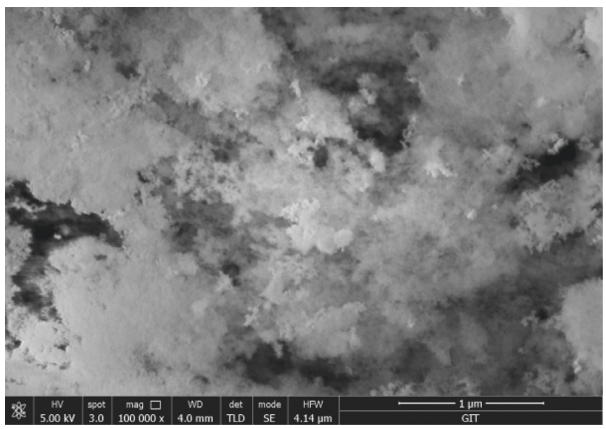

(a)

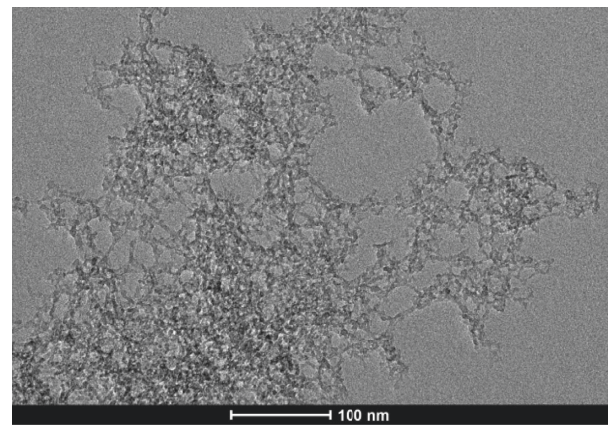

(b)

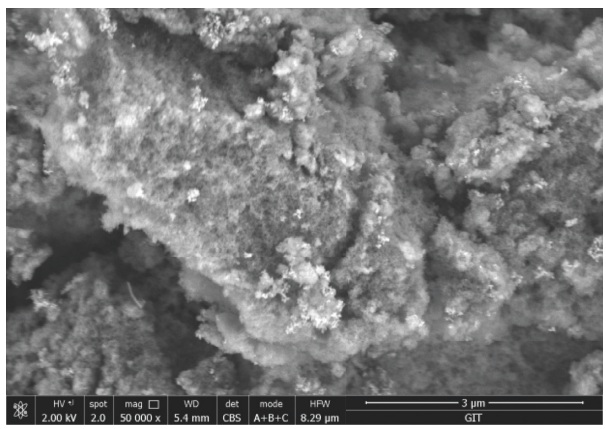

(c)

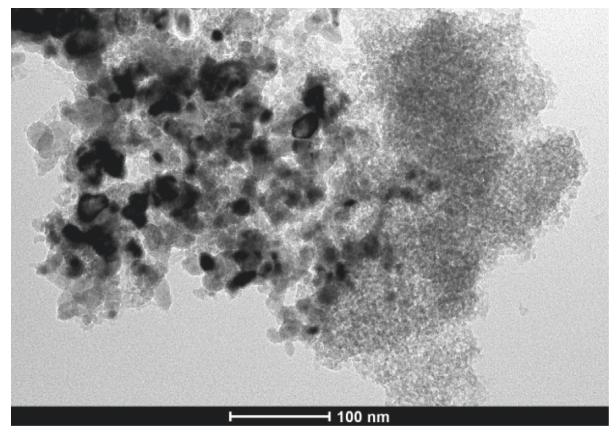

(d)

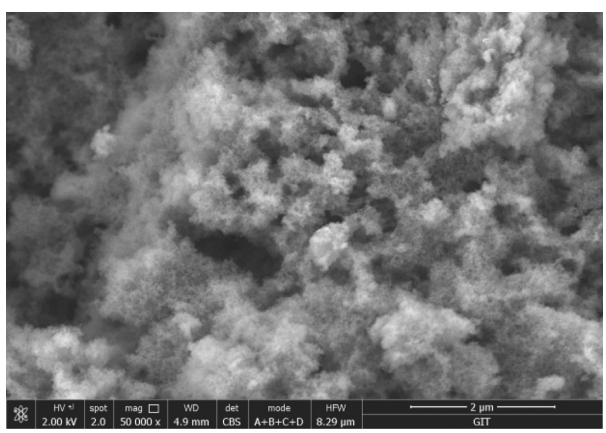

(e)

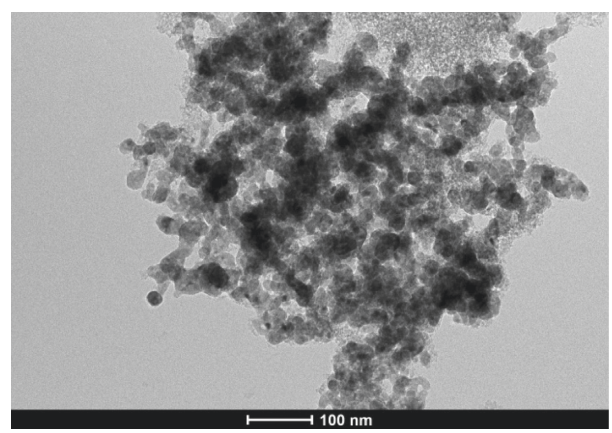

(f)

Figure 2: Continued.

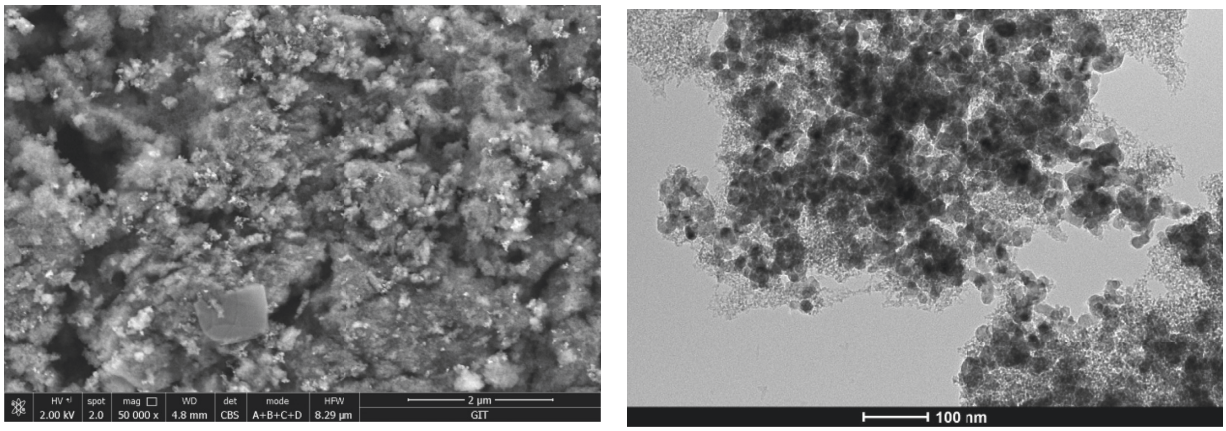

(g) (h)

Figure 2: SEM and TEM images of TiN@SiO_2 composite aerogels before and after thermal treatment: SEM (a) and TEM (b) of TiN@SiO_2; SEM (c) and TEM (d) of 300-TiO_2@SiO_2; SEM (e) and TEM (f) of 500-TiO_2@SiO_2; SEM (g) and TEM (h) of 700-TiO_2@SiO_2.

(Figure 2(b)), which revealed a porous nanostructure built up of small nanoparticles of size about 10 nm. After thermal oxidation at 300°C for 2 h, the bonding between particles is relatively close by SEM (Figure 2(c)), and the particles grow and sinter slightly at high temperature from TEM with higher magnification (Figure 2(d)). With the increase of oxidation temperature to 500°C, the microstructures of the samples hardly changed compared to 300-TiO_2@SiO_2 (see Figures 2(e) and 2(f)). However, when the oxidation temperature is further increased to 700°C, it can be observed that serious sintering phenomena with the number of large particles increase obviously (see Figures 2(g) and 2(h)). This trend is consistent with the previous BET results. When calcined at less than 500°C, the specific surface area of the material increases gradually due to the volatilization and pore expansion of residual ethanol in the aerogel. However, when the calcination temperature is up to 700°C, the specific surface area of the material begins to decrease due to the strong sintering effect.

3.2. Photocatalytic Activity of $TiO_{2-x}N_x$@SiO_2 Aerogels. As is well known, RhB as an organic dye existed in water can cause serious water pollution problems [24]. In this work, the RhB was chosen as model molecules to investigate the adsorption/photocatalytic activity of $TiO_{2-x}N_x$@SiO_2 composite aerogels. The adsorption/photocatalytic degradation efficiency is a combination effect of adsorption and photodegradation. Figure 3 shows the adsorption/photocatalytic degradation efficiency (η) curves of $TiO_{2-x}N_x$@SiO_2 composite aerogels for RhB under visible light irradiation. It can be found that the η values for RhB increases with the extension of reaction time, and the 500-TiO_2@SiO_2 composite aerogel exhibits the best adsorption/photocatalytic degradation rate for RhB, which obtained about 80% of the degradation rate in 30 min under visible light and over 95% after 120 min. For the as-prepared TiN@SiO_2, the adsorption/photocatalytic degradation rate quickly reached about 60% in the first 30 minutes due to the strong adsorption capacity of aerogel, and it hardly

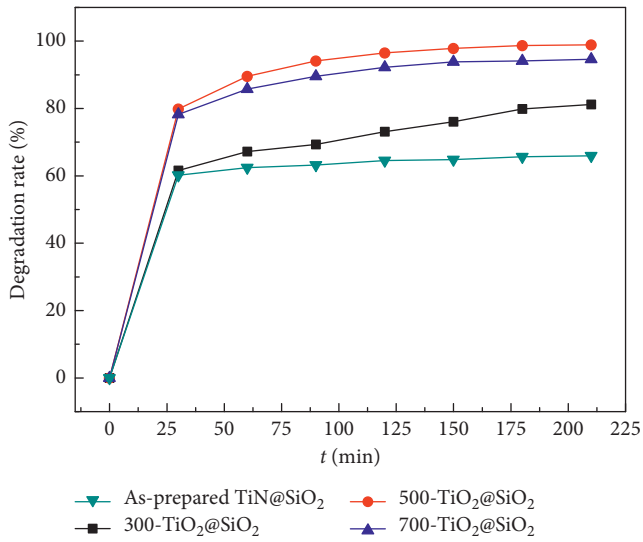

Figure 3: Adsorption/photocatalytic degradation rate curves of $TiO_{2-x}N_x$@SiO_2 composite aerogels for RhB under visible light irradiation.

increases with the increase of reaction time. According to previous BET analysis results, the mesoporous structure with higher pore volume of as-prepared TiN@SiO_2 composite aerogel is favorable for physical adsorption of RhB. Similar to as-prepared TiN@SiO_2, the adsorption/photocatalytic degradation rate of the 300-TiO_2@SiO_2 also quickly reached about 62% in the first 30 minutes, but it increases slowly with the increase of reaction time. This indicates that the as-prepared TiN@SiO_2 composite aerogel has almost no visible-light photocatalytic activity, while the 300-TiO_2@SiO_2 has very weak visible photocatalytic activity. Furthermore, as the oxidation temperature increases, the adsorptivity capacity of 500-TiO_2@SiO_2 and 700-TiO_2@SiO_2 aerogels is significantly increased after heat treatment because of the improved hydrophilicity of TiN@SiO_2 composite aerogel in the heat treatment process.

3.3. Possible Photocatalytic Reaction Mechanism of $TiO_{2-x}N_x@SiO_2$ Aerogels. To obtain the possible photocatalytic reaction mechanism of $TiO_{2-x}N_x@SiO_2$ aerogels, the phase composition, thermal stability, surface group, and absorbance properties as the increase of oxidation temperature were characterized by XRD, TG-DSC, FT-IR, and UV-Vis spectroscopy, respectively.

Figure 4 shows the XRD patterns of $TiN@SiO_2$ composite aerogels and TiN powers with different oxidation temperature. From Figure 4(a), it can be seen that all the samples have a dispersion characteristic peak at 15°–30°, which indicates that these samples are mainly amorphous with a relatively low crystallinity. This is consistent with the results of SEM and TEM. For the as-prepared $TiN@SiO_2$ composite aerogel, the reflections at 2θ angles of 36.8°, 42.7°, and 62.0° belong to (111), (200), and (220) crystal face of NaCl-type structure of TiN (JCPDS card number 38-1420). As the oxidation temperature increases to 300°C, there is no obvious change between the as-prepared $TiN@SiO_2$ and 300-$TiO_2@SiO_2$ composite aerogel, and only the characteristic diffraction peaks corresponding to the (111), (200), and (220) crystal faces of TiN are presented. According to previous work [25], this can be explained that the oxidation of TiN at 300°C is very weak, and its significant initial oxidation temperature is about 350°C. When the oxidation temperature is above 500°C, the characteristic diffraction peaks of TiN are completely disappeared, and two very weak and dispersion diffraction peaks at 25.4° and 54.4° which belong to the (101) and (211) crystal faces of anatase-TiO_2 appear. Comparing 500-$TiO_2@SiO_2$ with 700-$TiO_2@SiO_2$ samples, it can be found that the intensity of (101) crystal plane of 700-$TiO_2@SiO_2$ is slightly strong than that of 500-$TiO_2@SiO_2$. This indicates that the $TiO_{2-x}N_x@SiO_2$ aerogels have an excellent thermal stability.

Figure 4(b) gives the XRD patterns of pure TiN powers after oxidation at 500°C and 700°C. It can be seen that the pure TiN powers convert to anatase and rutile TiO_2 after oxidation at above 500°C. The TiO_2 by calcined TiN powers has a series of obvious diffraction peaks with relatively narrow and acuity. Halo peaks or other signs of amorphous phases are not observed, which implies that the crystal phase structures of TiO_2 are relatively complete with a high crystallinity. It is noteworthy that the (101) and (200) reflections at 2θ angles of 25.4° and 48.2° of anatase-TiO_2 are more pronounced than (110) and (211) peaks at 27.5° and 54.4° of rutile TiO_2 for oxidation at 500°C, respectively. But the case of the 700°C oxidation is just the opposite. This is due to the fact that other crystalline TiO_2 is easily transformed into more stable rutile structure at high temperatures [26]. The results are very different from $TiO_{2-x}N_x@SiO_2$ aerogels, because there are only weak and dispersed diffraction peaks of anatase TiO_2 observed in the latter. Considering the TiN wt.% of $TiN@SiO_2$ composite aerogels as 10%, the theoretical TiO_2 wt.% of $TiO_{2-x}N_x@SiO_2$ composite aerogels obtained by oxidation is 12.5%. The value is much higher than the detection limit of XRD. It means that the SiO_2 aerogels can significantly inhibit the phase transition of TiO_2 and the nano-TiO_2 can be highly dispersed in the SiO_2 aerogels.

From the XRD results, it seems that TiN in the $TiN@SiO_2$ composite aerogels can be completely oxidized to TiO_2 above 500°C. However, it is well known that pure TiO_2 has good photocatalytic activity only under ultraviolet irradiation, which is inconsistent with our experimental results. To further illustrate the visible light photocatalytic activity and thermal stability of $TiO_{2-x}N_x@SiO_2$ aerogels, TG-DTA experiments were carried out with as-prepared SiO_2 aerogel and as-prepared $TiN@SiO_2$ composite aerogel, as shown in Figure 5. From Figure 5(a), pure SiO_2 aerogel has a small weight loss (about 5%) from room temperature to 215°C which is attributed to desorption of physical adsorption water. Then, a notable weight loss (about 15%) is observed from 215°C to 310°C, which is attributed to the residual organic solvents in the aerogel. In the DTA curve, the decomposition of organic residues is reciprocated by the appearance of a remarkable endothermic peak with the maximum peak temperature (T_{max}) of 245°C. Further weight loss (about 7.5%) is observed at a temperature range of 310–750°C. This might be ascribed to the organic macromolecular formed by condensation of organic solvents during supercritical drying and further condensation of free –OH groups on the SiO_2 network to form Si–O–Si bridges [27]. The TG curve of $TiN@SiO_2$ composite aerogel is similar to that of as-prepared SiO_2 on the whole (see Figure 5(b)). About 5% of weight loss belongs to the physical adsorption water at a temperature range of room temperature –250°C. A sharp weight loss (about 5%) of the residual organic solvents at a temperature range of 250–290°C is also observed, which shows a remarkable endothermic peak with T_{max} of 258°C in the corresponding DTA curve. However, there is obvious difference that the $TiN@SiO_2$ composite aerogel has a broad endothermic peak at a temperature range of 290–570°C with T_{max} of 512°C in the DTA curve, which should be attributed to the gradual oxidation of TiN in the SiO_2 aerogel. It indicates that the $TiN@SiO_2$ needs to be completely oxidized above 570°C to form the $TiO_2@SiO_2$. According to our previous works about the oxidation of TiN coatings [25], the oxidation of TiN coating can be divided into three stages: mild oxidation below 500°C, moderate oxidation between 550 and 600°C, and severe oxidation between 650 and 750°C. Specifically, initial oxidation of TiN with a partial color change occurs at 350°C and remarkable oxidation of TiN occurs between 400 and 450°C. Therefore, if the oxidation temperature is selected properly, the N-doped $TiO_{2-x}N_x@SiO_2$ aerogel can be obtained by simple $TiN@SiO_2$ aerogel oxidation.

Figures 6(a) and 6(b) present the FT-IR and UV-Vis spectra of $TiN@SiO_2$ composite aerogels with different oxidation temperature, respectively. From Figure 6(a), the bands at about 1640 cm^{-1} and 3450 cm^{-1} can be assigned to the bending and stretching vibrations of the O-H groups, respectively. This is mainly due to the hydrophilicity of aerogels prepared by supercritical drying, which makes it easy to absorb water and form surface hydroxyl groups. According to the results of Huang et al. [28], the hydroxyl groups and hydrogen bonds on the surface of aerogels could enhance its adsorption capacity for RhB; thus, it will facilitate the subsequent photocatalytic degradation. The peaks

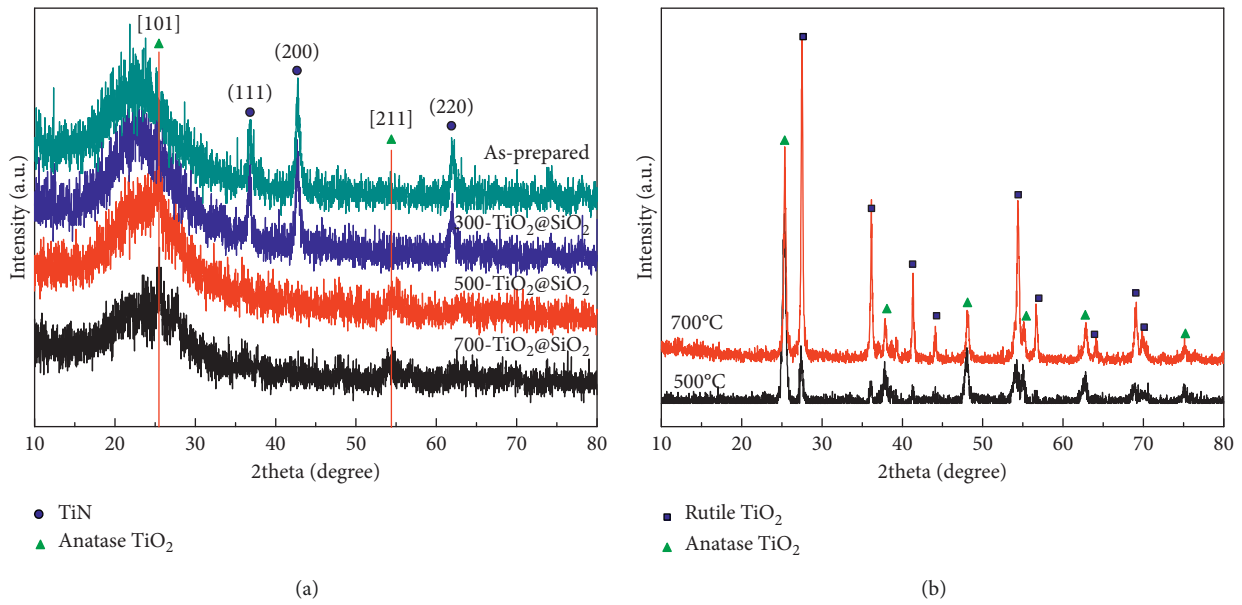

Figure 4: XRD patterns of $TiN@SiO_2$ composite aerogels (a) and TiN powers with different oxidation temperatures (b).

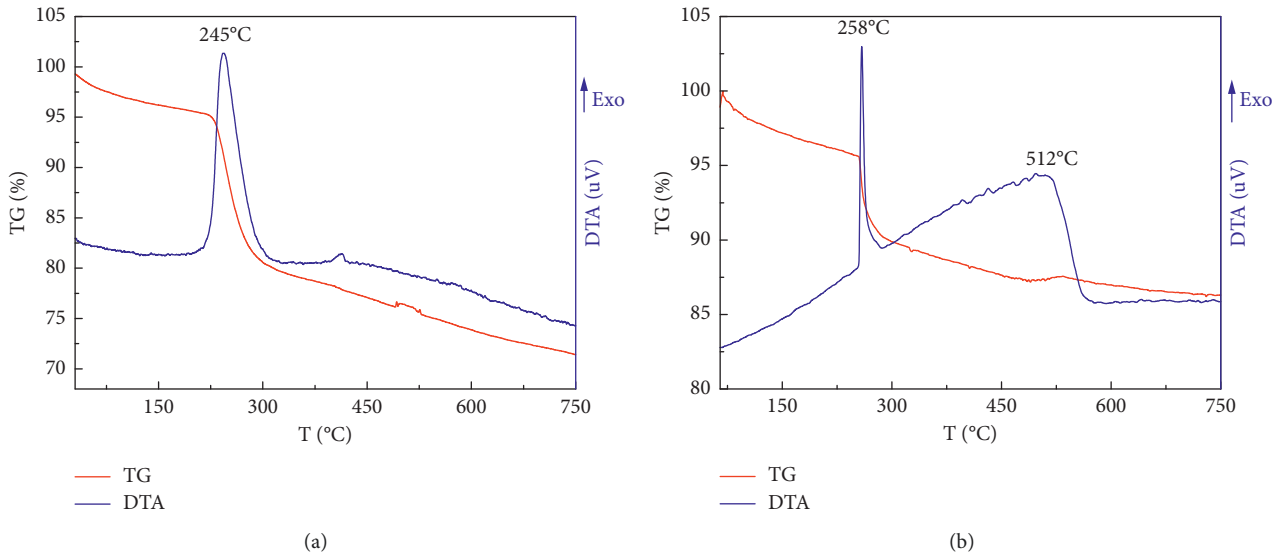

Figure 5: TG-DTA curves of SiO_2 aerogel (a) and $TiN@SiO_2$ composite aerogels (b).

assignable to symmetrical and asymmetrical stretching of Si-O-Si vibrations from the silica framework can be seen at 790–815 cm^{-1} and 1080–1100 cm^{-1}, respectively. It should be noted that there is the hetero-linkage Ti-O-Si bond at 940–960 cm^{-1} which indicates the incorporation of TiO_2 into SiO_2 to form binary TiO_2-SiO_2 systems. However, the expected Ti-N absorption bands (950–1000 cm^{-1}, 1100 cm^{-1} and 1300 cm^{-1}) [29] could not be observed because they were obscured by the strong absorptions bands in the region 950–1300 cm^{-1} from the silica framework. From Figure 6(b), the raw material SiO_2 aerogel exhibits almost no absorption from 300 to 800 nm. However, unlike pure TiO_2, which has no visible light absorption, the absorption of the $TiN@SiO_2$ composite aerogels becomes more obvious visible light absorption (>400 nm). And the increasing order of visible light absorption intensity with different oxidation temperatures is 300-$TiO_2@SiO_2$, 700-$TiO_2@SiO_2$, 500-$TiO_2@SiO_2$.

Based on the above discussion and experimental results, it can be inferred that the possible reasons of highest efficiency of 500-$TiO_2@SiO_2$ composite aerogel are as follows: Firstly, it has the highest specific surface area of all samples. Secondly, N-doping can be formed by incomplete oxidation for the 500-$TiO_2@SiO_2$ composite aerogel, and the content of N-doped is moderate for photocatalysis. Moreover, the 500-$TiO_2@SiO_2$ composite aerogel exhibits the best visible light absorption after oxidation. It can also draw a schematic picture of the mechanism connected to the interaction of $TiO_{2-x}N_x@SiO_2$ aerogels under visible light, as shown in Figure 7. $TiN@SiO_2$ composite aerogel is oxidized to $TiO_{2-x}N_x@SiO_2$ aerogel at a certain temperature under air

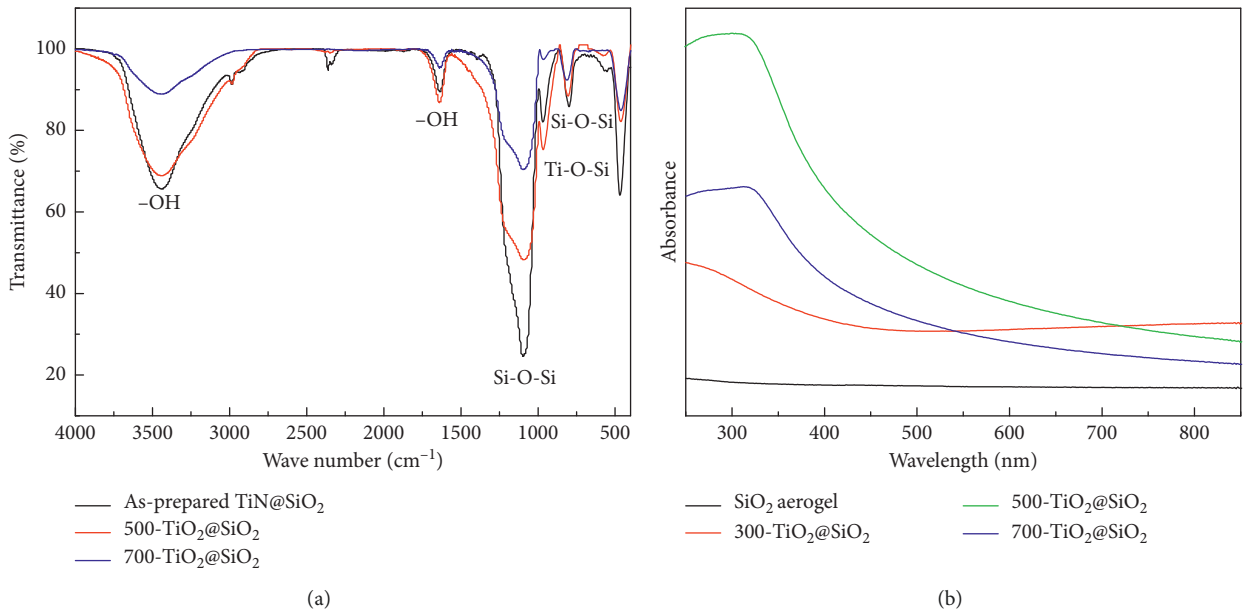

Figure 6: FT-IR (a) and UV-Vis (b) spectra of TiN@SiO$_2$ composite aerogels with different oxidation temperature.

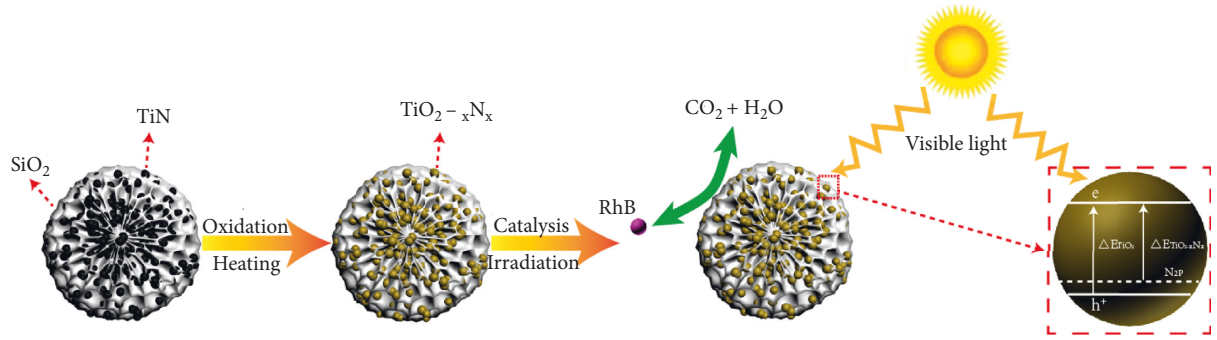

Figure 7: Sketch of the proposed mechanism for the processes induced by visible light irradiation of the $TiO_{2-x}N_x$@SiO_2 aerogels.

atmosphere; the reaction is shown in equation (1). Theoretically, if the oxidation temperature and time are chosen properly, the N-doped TiO_2@SiO_2 aerogels can be obtained due to the incomplete oxidation. Irradiation with visible light promotes the formation of the active oxygen species such as superoxide radicals and hydroxyl radicals [30, 31]. Numerous studies have shown that hydroxyl radicals are highly oxidative species which are considered to be the main species responsible for the photodegradation of the organic contaminants either adsorbed on the surface of the photocatalyst or in the bulk solution [32–34]. Therefore, the photocatalytic reaction can completely oxidize the RhB to form CO_2 and H_2O, as shown in equation (2). In fact, two effects must be considered with the final degradation efficiency when porous materials used as catalyst, the adsorption and degradation of the degradants. TiO_2 powers have a weak adsorption capacity, but SiO_2 aerogels can provide more adsorption centers; thus TiO_2@SiO_2 aerogels combine the advantage of high surface area and porous SiO_2 aerogels and semiconductor properties of TiO_2 to significantly yield novel materials appropriate for heterogeneous photocatalysis. When the N atoms get into the skeleton of TiO_2@SiO_2 aerogels to form the N-doped TiO_2@SiO_2 aerogels, a blue shift will appear with N-doped because not only is the top of the TiO_2 valence band lowered but the inserted N_{2p} levels are also lower in energy than the valence band of pure TiO_2; thus, the N-doped TiO_2@SiO_2 aerogels have a higher visible light active properties [33]:

$$\mathrm{TiN(s) + O_2(g) \longrightarrow TiO_{2-x}Nx(s)} \quad (2)$$

$$\mathrm{RhB + TiO_{2-x}Nx@SiO_2 + visible\,light \longrightarrow CO_2 + H_2O} \quad (3)$$

4. Conclusions

To improve the photocatalytic efficiency of TiO_2, this work combines the excellent properties of aerogels and nanophotocatalysts to take full advantage of the huge specific surface area, high adsorption efficiency, and strong transmittance of SiO_2 aerogel and photocatalytic activity of nanosized N-doped TiO_2 simultaneously. Sol-gel method,

supercritical drying, and direct oxidation process were adopted to prepare the nano-N-doped $TiO_2@SiO_2$ ($TiO_{2-x}N_x@SiO_2$, $0 \le x \le 2$) composite aerogels. The specific surface areas of all $TiO_{2-x}N_x@SiO_2$ samples exceeded 700 m^2/g and exhibited a honeycomb porous structure with fine particulate morphology. The 500-$TiO_2@SiO_2$ composite aerogel exhibits the best adsorption/photocatalytic degradation rate for RhB, which obtained about 80% of the degradation rate in 30 min under visible light and over 95% after 120 min. Furthermore, as the increase of oxidation temperature, the adsorptivity capacity of 500-$TiO_2@SiO_2$ and 700-$TiO_2@SiO_2$ aerogels is significantly increased after heat treatment because of the improved hydrophilicity of $TiN@SiO_2$ composite aerogel after air treatment. The SiO_2 aerogels can significantly inhibit the phase transition of TiO_2, and the nano-TiO_2 can be highly dispersed in the SiO_2 aerogels. If the oxidation temperature is selected properly, the N-doped $TiO_{2-x}N_x@SiO_2$ aerogel can be obtained by simple oxidation of $TiN@SiO_2$ aerogel.

Data Availability

All data included in this study are available upon request by contact with the corresponding author.

Conflicts of Interest

The authors declare that they have no conflicts of interest.

Acknowledgments

This research was supported by the National Natural Science Foundation of China (No. 2176605), S&T Plan Project Approving in Guizhou (Nos. Qiankehe LH Zi[2016] 7104, Qiankehe SY Zi[2014] 3058, and Qiankehe Jichu[2019] 1135), Natural Science Foundation of Guizhou Provincial Department of Education (Qiankehe KY Zi[2016]014), Science and Technology Services for Rural Industrial Revolution and Poverty Alleviation and Undergraduate Training Programs for Innovation and Entrepreneurship.

References

[1] M. Qamar and M. Muneer, "A comparative photocatalytic activity of titanium dioxide and zinc oxide by investigating the degradation of vanillin," *Desalination*, vol. 249, no. 2, pp. 535–540, 2009.

[2] V. M. d. S. Rocha, M. d. G. Pereira, L. R. Teles, and M. O. d. G. Souza, "Effect of copper on the photocatalytic activity of semiconductor-based titanium dioxide (anatase) and hematite (α-Fe_2O_3)," *Materials Science and Engineering: B*, vol. 185, pp. 13–20, 2014.

[3] V. Madhavi, P. Kondaiah, and G. Mohan Rao, "Influence of silver nanoparticles on titanium oxide and nitrogen doped titanium oxide thin films for sun light photocatalysis," *Applied Surface Science*, vol. 436, pp. 708–719, 2018.

[4] Y. Ban and X. Wang, "Features and application of titanium dioxide thin films in water treatment," *Procedia Engineering*, vol. 24, no. 3-4, pp. 663–666, 2011.

[5] J. Zhang, Y. H. Wu, F. Xue et al., "Indirect preparation of titanium dioxide oxidation plating layer as photoelectrode used in dye-sensitized solar cells," *Advanced Materials Research*, vol. 953-954, pp. 1095–1098, 2014.

[6] M. Kitano, K. Tsujimaru, and M. Anpo, "Decomposition of water in the separate evolution of hydrogen and oxygen using visible light-responsive TiO_2 thin film photocatalysts: effect of the work function of the substrates on the yield of the reaction," *Applied Catalysis A: General*, vol. 314, no. 2, pp. 179–183, 2006.

[7] J. G. Li, C. C. Tang, D. Li et al., "Monodispersed spherical particles of brookite-type TiO_2: synthesis, characterization, and photocatalytic property," *Journal of the American Ceramic Society*, vol. 87, no. 7, pp. 1358–1361, 2010.

[8] R. Long, Y. Dai, and B. Huang, "Geometric and electronic properties of Sn-doped TiO_2 from first-principles calculations," *The Journal of Physical Chemistry C*, vol. 113, no. 2, pp. 650–653, 2009.

[9] D. Fan, S. Guo, H. Wang et al., "Enhancement of the visible light photocatalytic activity of C-doped TiO_2 nanomaterials prepared by a green synthetic approach," *The Journal of Physical Chemistry C*, vol. 115, no. 27, pp. 13285–13292, 2011.

[10] C. D. Valentin, E. Finazzi, G. Pacchioni et al., "N-doped TiO_2: theory and experiment," *Chemical Physics*, vol. 339, no. 1–3, pp. 44–56, 2007.

[11] M. L. Guo, X. D. Zhang, C. T. Liang et al., "Mechanism of visible photoactivity of F-doped TiO_2," *Chinese Physics Letters*, vol. 27, no. 5, pp. 204–207, 2010.

[12] C. Yan, W. Yi, H. Yuan, X. Wu, and F. Li, "A highly photoactive S, Cu-codoped nano-TiO_2 photocatalyst: synthesis and characterization for enhanced photocatalytic degradation of neutral red," *Environmental Progress & Sustainable Energy*, vol. 33, no. 2, pp. 419–429, 2014.

[13] D. Pang, L. Qiu, Y. Wang, R. Zhu, and F. Ouyang, "Photocatalytic decomposition of acrylonitrile with N-F codoped TiO_2/SiO_2 under simulant solar light irradiation," *Journal of Environmental Sciences*, vol. 33, pp. 169–178, 2015.

[14] C. Zhang, Y. Zhou, J. Bao et al., "Hierarchical honeycomb Br-, N-codoped TiO_2 with enhanced visible-light photocatalytic H_2 production," *ACS Applied Materials & Interfaces*, vol. 10, no. 22, pp. 18796–18804, 2018.

[15] Q. Guo, Z. Zhang, X. Ma et al., "Preparation of N,F-codoped TiO_2 nanoparticles by three different methods and comparison of visible-light photocatalytic performances," *Separation and Purification Technology*, vol. 175, pp. 305–313, 2017.

[16] Y. D. Hou, X. C. Wang, L. Wu et al., "N-Doped SiO_2/TiO_2 mesoporous nanoparticles with enhanced photocatalytic activity under visible-light irradiation," *Chemosphere*, vol. 72, no. 3, pp. 414–421, 2008.

[17] M. Mahato, S. Mukherjee, and T. Mishra, "Development of magnetically separable mesoporous N doped TiO_2-SiO_2 coated Fe_3O_4 nanomaterial as solar photocatalyst for environmental application," *Materials Research Express*, vol. 6, no. 10, Article ID 105544, 2019.

[18] L. Wu, Y. Zhou, W. Nie, L. Song, and P. Chen, "Synthesis of highly monodispersed teardrop-shaped core-shell SiO_2/TiO_2 nanoparticles and their photocatalytic activities," *Applied Surface Science*, vol. 351, pp. 320–326, 2015.

[19] J. Gross, G. Reichenauer, and J. Fricke, "Mechanical properties of SiO_2 aerogels," *Meat Science*, vol. 36, no. 1-2, pp. 203–237, 2000.

[20] C. Sheng, W. Cheng, X. Shen et al., "Mesoporous amine-modified SiO_2 aerogel: a potential CO_2 sorbent," *Energy & Environmental Science*, vol. 4, no. 6, pp. 2070–2074, 2011.

[21] J.-M. Wang, "Preparation and properties of SiO_2 aerogel and fabric composite based on polyurethane," *Integrated Ferroelectrics*, vol. 189, no. 1, pp. 36–43, 2018.

[22] T. Y. Wei, T. F. Chang, S. Y. Lu, and Y.-C. Chang, "Preparation of monolithic silica aerogel of low thermal conductivity by ambient pressure drying," *Journal of the American Ceramic Society*, vol. 90, no. 7, pp. 2003–2007, 2010.

[23] G. Yin, C. Geng, Z. We et al., "Influence of supercritical drying fluids on structures and properties of low-density Cu-doped SiO_2 composite aerogels," *Journal of Sol-Gel Science and Technology*, vol. 69, no. 2, pp. 407–411, 2014.

[24] L. Hu, H. Yuan, L. Zou, F. Chen, and X. Hu, "Adsorption and visible light-driven photocatalytic degradation of Rhodamine B in aqueous solutions by Ag@AgBr/SBA-15," *Applied Surface Science*, vol. 355, pp. 706–715, 2015.

[25] S. Tang, J. Wang, Q. Zhu, Y. Chen, and X. Li, "Oxidation behavior of CVD star-shaped TiN coating in ambient air," *Ceramics International*, vol. 41, no. 8, pp. 9549–9554, 2015.

[26] S. Tang, J. Wang, Q. Zhu, Y. Chen, and X. Li, "Preparation of rutile TiO_2 coating by thermal chemical vapor deposition for anticoking applications," *ACS Applied Materials & Interfaces*, vol. 6, no. 19, pp. 17157–17165, 2014.

[27] Y. N. Kim, G. N. Shao, S. J. Jeon, S. M. Imran, P. B. Sarawade, and H. T. Kim, "Sol-gel synthesis of sodium silicate and titanium oxychloride based TiO_2-SiO_2 aerogels and their photocatalytic property under UV irradiation," *Chemical Engineering Journal*, vol. 231, pp. 502–511, 2013.

[28] X. Huang, J.-X. Liu, F. Shi, L. Yu, and S.-H. Liu, "Ambient pressure drying synthesis of Cs0.33WO3/SiO_2 composite aerogels for efficient removal of Rhodamine B from water," *Materials & Design*, vol. 110, pp. 624–632, 2016.

[29] K. Nakamoto, *Infrared and Raman Spectra of Inorganic and Coordination compounds*, Wiley, New York, NY, USA, fourth edition, 1986.

[30] J. Pan and S. P. Jiang, "Synthesis of nitrogen doped faceted titanium dioxide in pure brookite phase with enhanced visible light photoactivity," *Journal of Colloid and Interface Science*, vol. 469, pp. 25–30, 2016.

[31] S. Livraghi, M. C. Paganini, E. Giamello, A. Selloni, C. Di Valentin, and G. Pacchioni, "Origin of photoactivity of nitrogen-doped titanium dioxide under visible light," *Journal of the American Chemical Society*, vol. 128, no. 49, pp. 15666–15671, 2006.

[32] N. T. Nolan, D. W. Synnott, M. K. Seery, S. J. Hinder, A. Van Wassenhoven, and S. C. Pillai, "Effect of N-doping on the photocatalytic activity of sol-gel TiO_2," *Journal of Hazardous Materials*, vol. 211-212, pp. 88–94, 2012.

[33] G. Barolo, S. Livraghi, M. Chiesa, M. C. Paganini, and E. Giamello, "Mechanism of the photoactivity under visible light of N-doped titanium dioxide. Charge carriers migration in irradiated N-TiO_2 investigated by electron paramagnetic resonance," *The Journal of Physical Chemistry C*, vol. 116, no. 116, pp. 20887–20994, 2012.

[34] S. Yang and G. Lian, "New method to prepare nitrogen-doped titanium dioxide and its photocatalytic activities irradiated by visible light," *Journal of the American Ceramic Society*, vol. 87, no. 9, pp. 1803–1805, 2010.